# Radical Pathway in Catecholase Activity with Zinc-Based Model Complexes of Compartmental Ligands

Averi Guha,[†] Tanmay Chattopadhyay,[‡] Nanda Dulal Paul,[§] Madhuparna Mukherjee,[†] Somen Goswami,[†] Tapan Kumar Mondal,[||] Ennio Zangrando,*[,⊥] and Debasis Das*[,†]

[†]Department of Chemistry, University of Calcutta, 92, A. P. C. Road, Kolkata 700 009, India
[‡]Department of Chemistry, Panchokot Mahavidyalaya, Purulia, India
[§]Department of Inorganic Chemistry, Indian Association for the Cultivation of Science, Jadavpur, Kolkata 700 032, India
[||]Department of Chemistry, Jadavpur University, Jadavpur, Kolkata 700 032, India
[⊥]Dipartimento di Scienze Chimiche e Farmaceutiche, University of Trieste, Via L. Giorgieri 1, 34127 Trieste, Italy

Ⓢ *Supporting Information*

ABSTRACT: Four dinuclear and three mononuclear Zn^{II} complexes of phenol-based compartmental ligands (HL^1-HL^7) have been synthesized with the aim to investigate the viability of a radical pathway in catecholase activity. The complexes have been characterized by routine physicochemical studies as well as X-ray single-crystal structure analysis: $[Zn_2(H_2L^1)(OH)(H_2O)(NO_3)](NO_3)_3$ (**1**), $[Zn_2L^2Cl_3]$ (**2**), $[Zn_2L^3Cl_3]$ (**3**), $[Zn_2(L^4)_2(CH_3COO)_2]$ (**4**), $[Zn(HL^5)Cl_2]$ (**5**), $[Zn(HL^6)Cl_2]$ (**6**), and $[Zn(HL^7)Cl_2]$ (**7**) [L^1-L^3 and L^5-L^7 = 2,6-bis(R-iminomethyl)-4-methylphenolato, where R= *N*-ethylpiperazine for L^1, R = 2-(*N*-ethyl)pyridine for L^2, R = *N*-ethylpyrrolidine for L^3, R = *N*-methylbenzene for L^5, R = 2-(*N*-methyl)thiophene for L^6, R = 2-(*N*-ethyl)thiophene for L^7, and L^4 = 2-formyl-4-methyl-6-*N*-methylbenzene-iminomethyl-phenolato]. Catecholase-like activity of the complexes has been investigated in methanol medium by UV−vis spectrophotometric study using 3,5-di-*tert*-butylcatechol as model substrate. All complexes are highly active in catalyzing the aerobic oxidation of 3,5-di-*tert*-butylcatechol (3,5-DTBC) to 3,5-di-*tert*-butylbenzoquinone (3,5-DTBQ). Conversion of 3,5-DTBC to 3,5-DTBQ catalyzed by mononuclear complexes (**5**−**7**) is observed to proceed via formation of two enzyme−substrate adducts, ES1 and ES2, detected spectroscopically, a finding reported for the first time in any Zn^{II} complex catalyzed oxidation of catechol. On the other hand, no such enzyme−substrate adduct has been identified, and 3,5-DTBC to 3,5-DTBQ conversion is observed to be catalyzed by the dinuclear complexes (**1**−**4**) very smoothly. EPR experiment suggests generation of radicals in the presence of 3,5-DTBC, and that finding has been strengthened by cyclic voltammetric study. Thus, it may be proposed that the radical pathway is probably responsible for conversion of 3,5-DTBC to 3,5-DTBQ promoted by complexes of redox-innocent Zn^{II} ion. The ligand-centered radical generation has further been verified by density functional theory calculation.
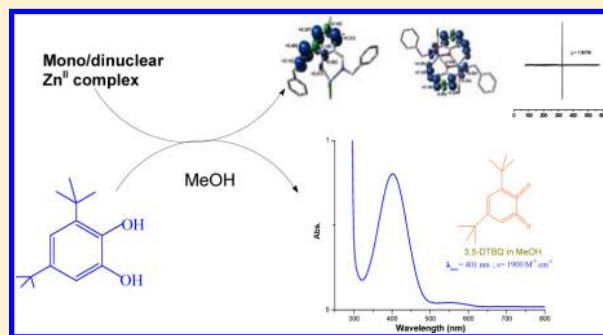
INTRODUCTION

Our current interest is addressed to study the mechanistic pathways of catechol oxidases, a member of type III copper proteins.[1] From the reports of distinguished research groups[1−10] and those from our laboratories,[11,12] it becomes evident that in the case of Cu^{II} and Mn^{III} metal-centered redox participation rather than a radical pathway is most probably responsible for the catecholase activity of these model compounds. The mechanism derived with copper(II) model compounds is rather convoluted, and literature often reports contradictory results.[1c,13−16] Encouraging observations[11,12,17,18] obtained with model compounds containing Cu^{II}, Ni^{II}, Mn^{III}, and Mn^{II} inspired us to investigate the activity of analogous Zn complexes as catechol oxidase models. Zinc ion, due to its redox-innocent character, should be an appropriate choice to investigate the viability of a radical pathway in catecholase-like

activity. It is noteworthy that a few interesting reports on the interactions of zinc center(s) with model substrates like 3,5-DTBC or TCC are in the literature.[19] However, to the best of our knowledge, no systematic study has yet been done on the catecholase-like activity of zinc complexes of phenol-based compartmental-type ligand systems. We are reporting herein the syntheses, characterization, and catecholase-like activity of seven Zn^{II} complexes, $[Zn_2(H_2L^1)(OH)(H_2O)(NO_3)](NO_3)_3$ (**1**), $[Zn_2L^2Cl_3]$ (**2**), $[Zn_2L^3Cl_3]$ (**3**), $[Zn_2(L^4)_2(CH_3COO)_2]$ (**4**), $[Zn(HL^5)Cl_2]$ (**5**), $[Zn(HL^6)Cl_2]$ (**6**), and $[Zn(HL^7)Cl_2]$ (**7**), of phenol-based compartmental Schiff-base ligands (Scheme 1) obtained by condensation of 2,6-diformyl-4-methylphenol with *N*-(2-aminoethyl)piperazine, (2-

Scheme 1. Compartmental Ligands Used in This Study
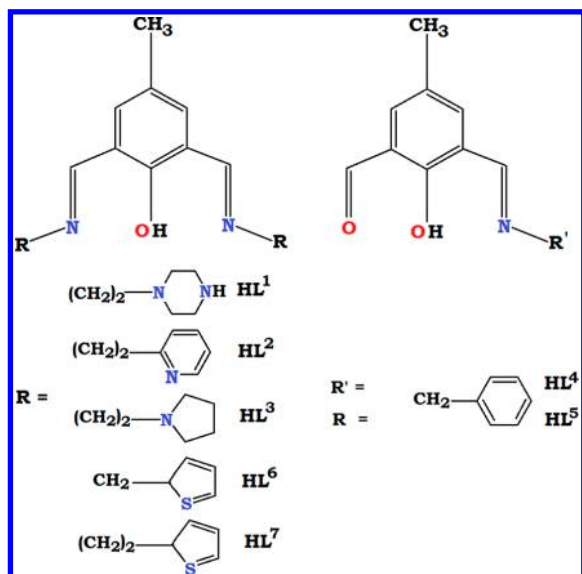
aminoethyl)pyridine, N-(2-aminoethyl)pyrrolidine, benzylamine, 2-thiophenemethylamine, and 2-thiopheneethylamine. Catecholase activity has been investigated using 3,5-di-tert-butylcatechol (3,5-DTBC) as model substrate. Our investigation suggests that the radical pathway rather than metal-centered redox participation is most probably responsible for oxidation of 3,5-DTBC to 3,5-di-tert-butylbenzoquinone (3,5-

DTBQ), the reaction known as catecholase activity, catalyzed by complexes of redox-innocent Zn^{II}.

■ EXPERIMENTAL SECTION

Physical Methods and Materials. All materials were obtained from commercial sources and used as purchased. Solvents were dried according to the standard procedure and distilled prior to use. 2,6-Diformyl-4-methylphenol was prepared according to the literature method.[20] Zinc chloride hexahydrate, zinc nitrate trihydrate, zinc acetate dihydrate (Merck), N-(2-aminoethyl)piperazine, (2-aminoethyl)pyridine, N-(2-aminoethyl)pyrrolidine, 2-thiopheneethylamine, 2-thiophenemethylamine, and benzylamine (Aldrich) were purchased from commercial sources and used as received. Elemental analyses (carbon, hydrogen, and nitrogen) were performed using a Perkin-Elmer 240C analyzer. Infrared spectra (4000−400 cm^{-1}) were recorded at 28 °C on a Shimadzu FTIR-8400S using KBr as a medium. Electronic spectra (800−200 nm) were obtained at 27 °C using a Shimadzu UV-3101 PC, where dry methanol was used as a medium as well as a reference. Electrospray mass spectra were recorded on a MICROMASS Q-TOF mass spectrometer. The electron paramagnetic resonance (EPR) experiment was done at both 25 and −135 °C in pure methanol using a Bruker EMX-X band spectrometer. Cyclic voltammograms were recorded in CH$_3$CN solutions containing 0.1 M TEAP at 25 °C using a three-electrode configuration (Pt working electrode, Pt counter electrode, Ag/AgCl reference) and a PC-controlled PAR model 273A electrochemistry system. ^{1}H NMR spectra (300 MHz) were recorded in the (CD$_3$)$_2$SO solvent on a Bruker AV300 Supercon NMR spectrometer using the solvent signal as the internal standard in a 5 mm BBO probe. Solution magnetic susceptibilities were measured by the Evans method[21] with a Bruker Avance DPX 300 spectrometer at 298 K. TMS was used as an internal reference in nonaqueous solutions, while a 2% solution of tertiary

Table 1. Crystallographic Data and Details of Refinement for Complexes 1−7

	1·2H$_2$O	2	3	4·H$_2$O	5	6	7
empirical formula	C$_{21}$H$_{42}$N$_{10}$O$_{17}$Zn$_2$	C$_{23}$H$_{23}$Cl$_3$N$_4$OZn$_2$	C$_{21}$H$_{31}$Cl$_3$N$_4$OZn$_2$	C$_{36}$H$_{36}$N$_2$O$_9$Zn$_2$	C$_{23}$H$_{22}$Cl$_2$N$_2$OZn	C$_{19}$H$_{18}$Cl$_2$N$_2$OS$_2$Zn	C$_{21}$H$_{22}$Cl$_2$N$_2$OS$_2$Zn
fw	837.39	608.54	592.59	771.41	478.70	490.74	518.80
cryst syst	orthorhombic	orthorhombic	orthorhombic	orthorhombic	monoclinic	monoclinic	monoclinic
space group	Pna2$_1$	Pbcn	P2$_1$2$_1$2$_1$	Pccn	P2$_1$/n	P2$_1$/c	P2$_1$/c
a (Å)	8.752(2)	25.599(3)	10.977(3)	15.7855(18)	9.3187(18)	9.2613(17)	8.3611(9)
b (Å)	40.166(9)	11.871(14)	18.852(5)	29.275(3)	11.670(2)	11.147(2)	24.085(3)
c (Å)	9.726(2)	16.507(15)	24.156(5)	8.7622(10)	20.982(4)	20.698(4)	11.7500(13)
β (deg)					100.744(3)	100.568(2)	106.4050(10)
V (Å^3)	3419.0(13)	5016.2(10)	4999(2)	4049.2(8)	2241.7(8)	2100.5(7)	2269.9(4)
Z	4	8	8	4	4	4	4
D$_{calcd}$, g cm^{-3}	1.627	1.612	1.575	1.265	1.418	1.552	1.518
μ(Mo Kα), mm^{-1}	1.490	2.256	2.261	1.234	1.350	1.634	1.517
F(000)	1736	2464	2432	1592	984	1000	1064
θ range (deg)	2.15−23.26	2.26−27.43	1.37−25.68	1.39−26.94	1.98−22.08	2.00−26.52	1.69−26.56
no. of reflns collcd	22 993	13 890	55 712	28 737	10 773	14 561	16 126
no. of indep reflns	3753	5414	9191	4245	2707	3994	4336
R$_{int}$	0.0634	0.0875	0.0520	0.0534	0.0737	0.0290	0.0230
no. of reflns (I > 2σ(I))	2302	2098	4486	2632	1769	3246	3562
no. of refined params	468	308	562	229	262	247	260
goodness-of-fit (F^2)	0.917	0.847	0.844	1.043	1.153	1.064	1.044
R1, wR2 (I > 2σ(I))^a	0.0424, 0.0931	0.0427, 0.0960	0.0479, 0.1094	0.0665, 0.2071	0.0938, 0.2522	0.0574, 0.1734	0.0374, 0.1062
residuals, e/Å^3	0.316, −0.235	0.392, −0.337	0.544, −0.384	0.638, −0.402	1.347, −1.833^b	1.351, −1.038^b	0.569, −0.562

^{a}R1 = Σ‖F$_o$| − |F$_c$‖/Σ|F$_o$|, wR2 = [Σw(F$_o^2$ − F$_c^2$)2/Σw(F$_o^2$)^2]$^{1/2}$. ^{b}Residuals close to the metal center or to the disordered thienyl ring.

butanol in CDCl$_3$ was used as the reference compound. Corrections for the susceptibility of the solvent and the difference in densities of the solvent and solution are ignored.[22] The diamagnetic correction to the molar susceptibility χ_m was calculated from Pascal's constants.[23]

X-ray Data Collection and Crystal Structure Determination. Crystal structure analyses of **1−3** were carried out on a Nonius DIP-1030H system, while data collections of **4−7** were performed on a Bruker Smart Apex diffractometer equipped with CCD. In all cases measurements were conducted at room temperature with Mo Kα radiation (λ = 0.71073 Å). Cell refinement, indexing, and scaling of the data sets were done using the programs Denzo and Scalepack,[24] Bruker Smart Apex, and Bruker Saint packages.[25] All structures were solved by direct methods and subsequent Fourier analyses[26] and refined by the full-matrix least-squares method based on F^2 with all observed reflections.[26] The Δ*F* map of **4** and **1** revealed the presence of one and two lattice water molecules, respectively, per complex unit. Hydrogen atoms were placed at calculated positions (of lattice water only H atoms of a molecule in **1** were located on the Fourier map). The ethyl chain C17−C18 in complex **2** was found disordered over two positions with refined occupancies of 0.712(16)/0.288(16). Compound **4** shows a void volume of 670.1 Å^3 (16.5% of the unit cell), but only a water molecule at half occupancy could be modeled as mentioned above. The C atoms of one thienyl fragment in **7** were isotropically refined with the ring disordered over two coplanar orientations of occupancies 0.533(5)/0.467(5).

All calculations were performed using the WinGX System, Ver 1.80.05.[27] Crystal data and details of refinements are given in Table 1.

Syntheses. *a.* **1**: *[Zn$_2$(H$_2$L^1)(OH)(H$_2$O)(NO$_3$)](NO$_3$)$_3$·2H$_2$O.* A methanolic solution (5 mL) of *N*-(2-aminoethyl)piperazine (0.258 g, 2 mmol) was added dropwise to a heated methanolic solution (10 mL) of 2,6-diformyl-4-methylphenol (0.164 g, 1 mmol), and the resulting mixture was boiled for 0.5 h. Then a methanolic solution (15 mL) of zinc nitrate trihydrate (0.885 g, 3 mmol) was added and the resulting mixture refluxed for another 2 h. After cooling, the clear yellow solution was kept in a CaCl$_2$ desiccator in the dark, and square-shaped yellow crystals, suitable for X-ray data collection were obtained after a few days. (Yield 65%). Anal. Calcd for C$_{21}$H$_{42}$N$_{10}$O$_{17}$Zn$_2$ (**1**): C, 30.12; H, 5.05; N, 16.73. Found: C, 30.04; H, 4.94; N, 16.66.

FT-IR *ν* (KBr) [cm^{-1}] = 3467.8(br), 1645.7(s), 1547.4(s), 1383.3(br).

^{1}H NMR (300 MHz, DMSO-d_6, 25 °C) δ = 8.345 (s, 2H, C=N), 7.319 (s, 2H, Ar), 3.876, 3.729, 3.698 (t, 4H, CH$_2$), 2.866−2.459 (m, 20H, CH$_2$), 2.155 (s, 3H, CH$_3$).

ESI-MS *m/z* = 723.57 (calcd for {[Zn$_2$(H$_2$L^1)(OH)(NO$_3$)$_3$] + H}$^+$: 722.3553).

b. **2**: *[Zn$_2$L^{2}Cl$_3$].* Complex **2** was prepared using the same procedure as for **1** where (2-aminoethyl)pyridine was used instead of *N*-(2-aminoethyl)piperazine (0.258 g, 2 mmol) and the metal salt zinc chloride hexahydrate (0.409 g, 3 mmol). (Yield 72%). Anal. Calcd for C$_{23}$H$_{23}$N$_4$OCl$_3$Zn$_2$ (**2**): C, 45.39; H, 3.81; N, 9.21. Found: C, 45.28; H, 3.74; N, 9.18.

FT-IR *ν* (KBr) [cm^{-1}] = 1683.0(s), 1598.2(s).

^{1}H NMR (300 MHz, DMSO-d_6, 25 °C) δ = 8.505 (s, 2H, C=N), 7.403−6.633 (s, 10H, Ar), 2.966−2.743 (m, 8H, CH$_2$), 2.295 (s, 3H, CH$_3$).

ESI-MS *m/z* = 573.34 (calcd for {[Zn$_2$L^{2}Cl$_2$] + H}$^+$: 574.1556).

c. **3**: *[Zn$_2$L^{3}Cl$_3$].* Complex **3** was prepared adopting a similar procedure as for **1** using *N*-(2-aminoethyl)pyrrolidine (0.228 g, 2 mmol) and zinc chloride hexahydrate (0.409 g, 3 mmol; yield 68%). Anal. Calcd for C$_{21}$H$_{31}$N$_4$OCl$_3$Zn$_2$ (**3**): C, 42.56; H, 5.27; N, 9.45. Found: C, 42.50; H, 5.19; N, 9.37.

FT-IR *ν* (KBr) [cm^{-1}] = 1643.3(s), 1547.6(s).

^{1}H NMR (300 MHz, DMSO-d_6, 25 °C) δ = 8.505 (s, 2H, C=N), 7.403 (s, 2H, Ar), 3.066−2.621 (m, 16H, CH$_2$), 2.196 (s, 3H, CH$_3$), 2.020−1.724 (m, 8H, CH$_2$).

ESI-MS *m/z* = 580.26 (calcd for {[Zn$_2$L^{3}Cl$_2$] + Na}$^+$: 580.1789).

d. **4**: *[Zn$_2$(L^4)$_2$(CH$_3$COO)$_2$]·H$_2$O.* Complex **4** was prepared adopting a similar procedure as for **1** using benzylamine (0.214 g, 2 mmol) and zinc acetate dihydrate (0.659 g, 3 mmol; yield 70%). Anal. Calcd for

C$_{36}$H$_{36}$N$_2$O$_9$Zn$_2$ (**4**): C, 56.05; H, 4.70; N, 3.63. Found: C, 55.94; H, 4.61; N, 3.57.

FT-IR *ν* (KBr) [cm^{-1}] = 3450.8(br), 1717.8(s), 1634.0(s), 1534.5(s), 1282.6(s).

^{1}H NMR (300 MHz, DMSO-d_6, 25 °C) δ = 10.459 (s, 1H, CHO), 8.274 (s, 1H, C=N), 7.306−6.805 (m, 7H, Ar), 2.674 (s, 4H, CH$_2$), 2.255 (s, 3H, CH$_3$).

ESI-MS *m/z* = 718.50 (calcd for {[Zn$_2$(L^4)$_2$] + Na}$^+$: 717.3969).

e. **5**: *[Zn(HL^5)Cl$_2$].* Complex **5** was prepared as above using benzylamine (0.214 g, 2 mmol) and zinc chloride hexahydrate (0.409 g, 3 mmol; yield 70%). Anal. Calcd for C$_{23}$H$_{22}$N$_2$OCl$_2$Zn (**5**): C, 57.70; H, 4.63; N, 5.85. Found: C, 57.61; H, 4.56; N, 5.78.

FT-IR *ν* (KBr) [cm^{-1}] = 1641.7(s), 1541.4(s).

^{1}H NMR (300 MHz, DMSO-d_6, 25 °C) δ = 8.274 (s, 2H, C=N), 7.306−6.805 (m, 7H, Ar), 2.674 (s, 2H, CH$_2$), 2.255 (s, 3H, CH$_3$).

ESI-MS *m/z* = 478.24 (calcd for {[Zn(HL^5)Cl] + Na + 2Li}$^+$: 480.1543).

f. **6**: *[Zn(HL^6)Cl$_2$].* Complex **6** was prepared by adopting a similar procedure as for **1** using 2-thiophenemethylamine (0.226 g, 2 mmol) and zinc chloride hexahydrate (0.409 g, 3 mmol; yield 75%). Anal. Calcd for C$_{19}$H$_{18}$N$_2$OS$_2$Cl$_2$Zn (**6**): C, 46.50; H, 3.70; N, 5.71. Found: C, 46.42; H, 3.63; N, 5.63.

FT-IR *ν* (KBr) [cm^{-1}] = 1636.3(s), 1542.2(s).

^{1}H NMR (300 MHz, DMSO-d_6, 25 °C) δ = 8.505 (s, 1H, C=N), 7.403−6.633 (m, 8H, Ar), 2.969 (s, 4H, CH$_2$), 2.295 (s, 3H, CH$_3$).

ESI-MS *m/z* = 477.33 (calcd for {[Zn(HL^6)Cl] + Na}$^+$: 478.3272).

g. **7**: *[Zn(HL^7)Cl$_2$].* Complex **7** was prepared by adopting a similar procedure as for **1** using 2-thiopheneethylamine (0.254 g, 2 mmol) and zinc chloride hexahydrate (0.409 g, 3 mmol; yield 72%). Anal. Calcd for C$_{21}$H$_{22}$N$_2$OS$_2$Cl$_2$Zn (**7**): C, 48.61; H, 4.27; N, 5.40. Found: C, 48.53; H, 4.19; N, 5.32.

FT-IR *ν* (KBr) [cm^{-1}] = 1638.4(s), 1541.5(s).

^{1}H NMR (300 MHz, DMSO-d_6, 25 °C) δ = 8.505 (s, 1H, C=N), 7.403−6.633 (m, 8H, Ar), 2.969−2.830 (m, 4H, CH$_2$), 2.295 (s, 3H, CH$_3$), 1.975−1.836 (m, 4H, CH$_2$).

ESI-MS *m/z* = 483.31 (calcd for {[Zn(HL^7)Cl] + H}$^+$: 484.3987).

Computational Details. Density functional theory (DFT) calculations were carried out with the Gaussian 03 package.[28] The exchange functional of Becke and the correlation functional of Lee, Yang, and Parr (B3LYP)[29,30] were employed. All elements except zinc were assigned the 6-31G(d) basis set. The Lanl2dz basis set with effective core potential was employed for the zinc atom.[24,31] Vibrational frequency calculations were performed to ensure that the optimized geometries represent the local minima and there are only positive eigen-values.

RESULTS AND DISCUSSION

Syntheses and Characterization. The Schiff-base ligands were synthesized through the classical condensation reaction between 2,6-diformyl-4-methylphenol and *N*-(2-aminoethyl)-piperazine, (2-aminoethyl)pyridine, *N*-(2-aminoethyl)-pyrrolidine, benzylamine, 2-thiophenemethylamine, and 2-thiopheneethylamine in methanol medium. The Schiff-base ligands on treatment with the zinc salts *in situ* gave us the seven complexes. Complexes were characterized by IR, ^{1}H NMR, and ESI-MS study (Supporting Information, Figures S1−S21). All complexes show bands due to the C=N stretch in the range 1630−1685 cm^{-1} and skeletal vibration in the range 1540−1598 cm^{-1}. Broad bands centered at 1380 cm^{-1} exhibited by **1** are due to the weakly coordinated NO$_5{}^{3-}$ ion. In **4** an additional band at 1283 cm^{-1} is due to acetate anion. Complexes **1** and **4** due to their coordinated water molecules show broad bands in the range 3450−3465 cm^{-1}. ^{1}H NMR of the complexes shows a singlet signal in the range δ ≈ 8.2−8.5 corresponding to the imine hydrogen, the peaks between δ 6.5 and 7.5 correspond to the aromatic hydrogens, two types of methylene hydrogens are in the range of δ ≈ 1.8−3.0 giving rise to a multiplet in **1, 2, 3,**

8752

dx.doi.org/10.1021/ic300400v | *Inorg. Chem.* 2012, 51, 8750−8759

and **7** and singlet in **4**−**6**, and the three hydrogens of the methyl group appear as a singlet between δ 2.1 and 2.7. ESI-MS study of complexes **1**−**7** in methanol show the most abundant peak called the base peak at 752.57, 573.34, 580.26, 716.53, 478.24, 477.33, and 483.31 amu, respectively. These results corroborate well with the respective monopositive species of formulation $\{[Zn_2(H_2L^1)(OH)(NO_3)_3] + H\}^+$, $\{[Zn_2L^2Cl_2] + H\}^+$, $\{[Zn_2L^3Cl_2] + Na\}^+$, $\{[Zn_2(L^4)_2] + Na\}^+$, $\{[Zn(HL^5)Cl] + Na + 2Li\}^+$, $\{[Zn(HL^6)Cl] + Na\}^+$, and $\{[Zn(HL^7)Cl] + H\}^+$. The isotopic distributions of the observed and simulated spectral patterns (Supporting Information, Figures S15−S21) are in good agreement with each other in all cases, suggesting the right assignment of the positive ions. Electronic spectra of all complexes were recorded in dry methanol. Two characteristic bands are observed in all spectra: one very intense band in the range 250−260 nm attributed to intraligand charge transfer and another low-energy low intensity band in the range 390−415 nm assigned to ligand to metal charge transfer (LMCT; either $PhO^-/X^- \rightarrow Zn^{II}$ or admixture of PhO^- and $X^- \rightarrow Zn^{II}$, where X = NO_3/OAc/Cl). In the case of complex **5** one shoulder at ∼448 nm is noticed probably originating from LMCT.

Description of Crystal Structure. X-ray structural characterization of the dinuclear complex **1** (Figure 1) discloses
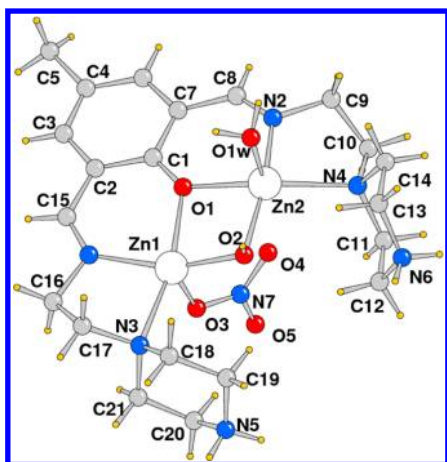

Figure 1. Molecular structure of the complex cation of **1**.

Table 2. Coordination Bond Distances (Angstroms) and Angles (degrees) for Complex 1

Zn(1)−O(1)	2.060(6)	Zn(2)−O(1)	2.052(7)
Zn(1)−O(2)	1.939(6)	Zn(2)−O(2)	1.975(5)
Zn(1)−O(3)	2.122(7)	Zn(2)−O(1w)	2.089(7)
Zn(1)−N(1)	2.033(8)	Zn(2)−N(2)	2.037(8)
Zn(1)−N(3)	2.238(7)	Zn(2)−N(4)	2.215(8)
Zn(1)−Zn(2)	3.0006(15)		
O(2)−Zn(1)−N(1)	158.2(3)	O(2)−Zn(2)−N(2)	163.7(3)
O(2)−Zn(1)−O(1)	82.7(2)	O(2)−Zn(2)−O(1)	82.1(2)
N(1)−Zn(1)−O(1)	85.6(3)	N(2)−Zn(2)−O(1)	85.5(3)
O(2)−Zn(1)−O(3)	100.0(3)	O(2)−Zn(2)−O(1w)	93.5(3)
N(1)−Zn(1)−O(3)	99.6(3)	N(2)−Zn(2)−O(1w)	98.6(3)
O(1)−Zn(1)−O(3)	96.6(3)	O(1)−Zn(2)−O(1w)	97.8(3)
O(2)−Zn(1)−N(3)	103.8(3)	O(2)−Zn(2)−N(4)	104.9(3)
N(1)−Zn(1)−N(3)	83.6(3)	N(2)−Zn(2)−N(4)	83.0(3)
O(1)−Zn(1)−N(3)	164.7(3)	O(1)−Zn(2)−N(4)	157.3(3)
O(3)−Zn(1)−N(3)	95.9(3)	O(1w)−Zn(2)−N(4)	103.2(3)
Zn(2)−O(1)−Zn(1)	93.7(3)	Zn(1)−O(2)−Zn(2)	100.1(3)

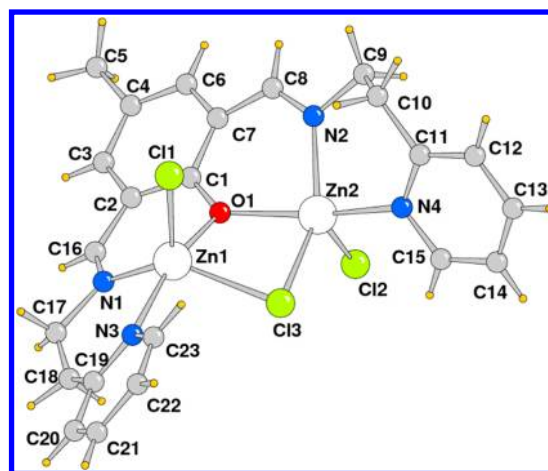**Figure 2.** Molecular structure of complex **2** (of the disordered C17−C18 fragment only that at higher occupancy is shown).

a distorted square pyramidal geometry for Zn ions. Basal plane positions are occupied by the doubly bridging μ-phenoxo and μ-hydroxido oxygen atoms, the L^1 imine−nitrogen and amine donor from the piperazine ring. Zn−N(piperazine) bond distances, of 2.238(7) and 2.215(8) Å, are significantly longer with respect to the Zn−N(imino) ones (mean 2.035(8) Å; Table 2). The metal ions, separated by 3.0006(15) Å, are slightly displaced by −0.45(1) and 0.23(1) Å from the phenolato mean plane toward the apical position. The piperazine moieties attain a chair conformation, and the protonated uncoordinated amine nitrogens, besides guaranteeing the electrical neutrality of the system, are engaged in a H-bonding scheme with nitrate anions and lattice water molecules.

The chloro-bridged complexes **2** (Figure 2) and **3**[32] have a similar structure. Each metal is coordinated by one μ-phenoxo oxygen, one μ-chlorine atom, the imine and pyridine (pyrrolidine in **3**) nitrogen atoms, and one chlorine, the latter at the apical position. The coordination bond distances are in line with those expected, but the Zn−N(pyridine) bond lengths

in **2** (Table 3) are slightly shorter than the Zn−N(pyrrolidine) ones of **3** (Table 4) for the different hybridization of the N donor. The square pyramidal geometry is highly distorted with a trigonal index[33] of 0.555 and 0.200 in **2** and in a range between 0.122 and 0.435 for the two independent complexes of **3**. Here the Zn−Cl$_{bridging}$ bond distances are longer compared to the Zn−Cl$_{apical}$ ones (mean value 2.40 vs 2.25 Å), and the intermetallic separation is ca. 3.40 Å. It is worth noting that in **2** and in the two complexes of **3** the zinc ions are considerably displaced from the phenolato mean plane by ca. 1.0 Å, likely compelled by coordination of the py and pyrrolidine ligands. Chloride anions significantly distort the planarity of the $[Zn_2L^2]$ framework in **2** and **3** with respect to the structures of similar complexes with carboxylate or hydroxide as coordinating anions.[34]

Complex **4** (Figure 3) is basically different from **1**−**3**. In fact, two unsymmetrical tridentate Schiff-base ligands, chelating the metal ions in a head−tail arrangement, form a phenoxido-bridged dimer located on a crystallographic inversion center. The metal possesses a square pyramidal coordination sphere

Table 3. Coordination Bond Distances (Angstroms) and Angles (degrees) for Complex 2

Zn(1)−O(1)	2.098(3)	2.097(4)	Zn(2)−O(1)	2.046(3)
Zn(1)−N(1)	2.058(4)	2.062(5)	Zn(2)−N(2)	2.066(4)
Zn(1)−N(3)	2.175(4)	2.172(5)	Zn(2)−N(4)	2.115(4)
Zn(1)−Cl(1)	2.2695(16)	2.2698(18)	Zn(2)−Cl(2)	2.2518(17)
Zn(1)−Cl(3)	2.4221(16)	2.4219(17)	Zn(2)−Cl(3)	2.5141(15)
Zn(1)−Zn(2)	3.4028(10)	3.4023(11)		
N(1)−Zn(1)−O(1)	85.06(17)	85.06(18)	O(1)−Zn(2)−N(2)	85.55(15)
N(1)−Zn(1)−N(3)	89.89(18)	89.9(2)	O(1)−Zn(2)−N(4)	153.90(17)
O(1)−Zn(1)−N(3)	163.74(15)	163.70(17)	N(2)−Zn(2)−N(4)	91.69(17)
N(1)−Zn(1)−Cl(1)	124.93(16)	125.00(18)	O(1)−Zn(2)−Cl(2)	103.70(11)
O(1)−Zn(1)−Cl(1)	96.33(10)	96.35(12)	N(2)−Zn(2)−Cl(2)	111.04(13)
N(3)−Zn(1)−Cl(1)	99.23(13)	99.24(14)	N(4)−Zn(2)−Cl(2)	101.51(15)
N(1)−Zn(1)−Cl(3)	130.46(16)	130.43(18)	O(1)−Zn(2)−Cl(3)	78.56(10)
O(1)−Zn(1)−Cl(3)	79.78(10)	79.84(11)	N(2)−Zn(2)−Cl(3)	141.89(13)
N(3)−Zn(1)−Cl(3)	91.94(13)	91.85(14)	N(4)−Zn(2)−Cl(3)	88.02(13)
Cl(1)−Zn(1)−Cl(3)	103.56(6)	103.56(6)	Cl(2)−Zn(2)−Cl(3)	106.32(6)
Zn(2)−O(1)−Zn(1)	110.36(14)	110.28(16)	Zn(1)−Cl(3)−Zn(2)	87.14(4)

(trigonal index 0.114) with two μ-phenoxido oxygens, an imine N donor, and a carbonyl oxygen located in the equatorial plane, the axial position being occupied by an acetate anion. All coordination bond lengths are comparable, ranging from 1.981(4) to 2.115(4) Å (Table 5), where surprisingly the shortest is relative to the apical Zn−O(acetate) bonds. The crystal packing shows a residual void corresponding to 16% of the unit cell volume (Figure 4), but only one lattice water molecule at half occupancy could be successfully refined.

Finally, 5−7 are mononuclear complexes (Figures 5−7), with the Zn ion tetrahedrally coordinated by the phenoxo oxygen, the imino nitrogen donor from the chelating ligand, and two chlorides. The coordination distances are comparable to those detected in the dinuclear species, and of these the Zn−Cl bond lengths (in a range from 2.2163(15) to 2.2360(8) Å, Table 6) are only slightly shorter than the singly bound chlorides in complexes 2 and 3. Interestingly, the imine nitrogen N2 is protonated in all these mononuclear compounds.

Catechol Oxidase Activity. The catalytic activity of 1−7 was pursued by treating 1×10^{-4} mol dm^{-3} complex solutions with 1×10^{-2} mol dm^{-3} of 3,5-DTBC. All four dinuclear complexes behave similarly in methanol, and Figure 8 shows the spectral change for 2 as representative. The reaction was monitored for 2 h after addition of 3,5-DTBC to the methanolic solution of the complex. Initially, complexes 1−4 show bands at ∼400 nm. Upon addition of 3,5-DTBC the spectral run done immediately exhibits increment of the absorbance nearly above that band. Since it is well established that 3,5-DTBQ shows band maxima at 400 nm in pure methanol, the experiment unequivocally proves oxidation of 3,5-DTBC to 3,5-DTBQ catalyzed by the dinuclear Zn^{II} complexes. The kinetics of the 3,5-DTBC oxidation was determined by monitoring the increase of the product 3,5-DTBQ. The experimental conditions were the same as we reported earlier.[11] All dinuclear complexes showed saturation kinetics where a treatment based on the Michaelis−Menten model seemed to be appropriate. The values of the Michaelis binding constant (K_m), maximum velocity (V_{max}), and rate constant for dissociation of substrates (i.e., turnover number, k_{cat}) were calculated for complexes from the graphs of $1/V$ vs $1/[S]$ (Figure 9), known as the Lineweaver−Burk graph using the equation $1/V = \{K_M/V_{max}\}\{1/[S]\} + 1/V_{max}$, and the kinetic parameters are presented in Table 7.

The catalytic behavior exhibited by mononuclear complexes 5−7 is very interesting. Figure 10 depicts the changes of the spectral behavior of complex 5 upon addition of 3,5-DTBC monitored up to 2 h course of reaction as representative. From Figure 10 it is clear that complex 5 shows band maxima at 393 nm with a shoulder at 448 nm. Both bands vanish immediately after addition of 3,5-DTBC, and two new bands develop at 360 and 448 nm. It is also evident that the band at 448 nm gradually decreases with concomitant increment of the band at 360 nm. It is obvious that none of the bands correspond to 3,5-DTBQ. Interestingly, after nearly 1 h reaction the spectrum obtained shows a clear indication of red shifting of the band toward 400 nm with concomitant decrement of the band at 360 nm, and the species showing $\lambda_{max} \approx 400$ nm is identified as 3,5-DTBQ. Thus, the catechol oxidations here promoted by the mononuclear complexes occur via formation of two stable intermediates having λ_{max} at 360 and 448 nm. We observed a similar catalytic reaction during oxidation of 3,5-DTBC catalyzed by our dicopper(II) complexes, where formation of 3,5-DTBQ took place via two intermediates ES1 and ES2.[11] It is worth noting that from the UV−vis spectral study only the binding modes of 3,5-DTBC cannot be guessed. To get a better understanding of the ES1 and ES2 structures, here we also performed a ESI-MS spectral study, as we did with our copper system, by selecting complex 5. Earlier we proposed the mono- and bidentate modes of coordination of 3,5-DTBC in ES1 and ES2 intermediates, respectively. In the present case, the ESI-MS spectrum obtained immediately after mixing our mononuclear complex 5 with 3,5-DTBC exhibits the main peak called the base peak at 657.50 amu which corroborates well with ES1 having a monodentate mode of coordination of 3,5-DTBC with the metal center with probable composition [Zn(HL^5)(3,5-DTBC$^-$) + Na + Li]$^+$ (m/z_{calcd} = 659.07 amu), and the ESI-MS spectrum obtained after 30 min of reaction shows a base peak at 343.34 amu corroborating well with ES2 where the bidentate mode of coordination of the substrate with the metal center has been predicted with probable composition [Zn(L^5)-(3,5-DTBC^{2-}) + 2Na^I + Li^I + Li]$^{2+}$ (m/z_{calcd} =343.99 amu) (Supporting Information, Figures S36 and S37). The isotopic distributions of the observed and simulated spectral pattern are in good agreement with each other in the case of ES1 and ES2, thereby suggesting the right assignment of the positive ions.

**Table 4. Coordination Bond Distances (Angstroms) and Angles (degrees) for Complex 3**

complex A		complex B	
Zn(1)−N(1)	2.044(7)	Zn(1b)−N(1b)	2.071(8)
Zn(1)−O(1)	2.082(6)	Zn(1b)−O(1b)	2.102(6)
Zn(1)−N(3)	2.211(7)	Zn(1b)−N(3b)	2.193(8)
Zn(1)−Cl(1)	2.237(2)	Zn(1b)−Cl(1b)	2.247(3)
Zn(1)−Cl(3)	2.359(3)	Zn(1b)−Cl(3b)	2.342(3)
Zn(2)−N(2)	2.040(9)	Zn(2b)−O(1b)	2.070(6)
Zn(2)−O(1)	2.062(6)	Zn(2b)−N(2b)	2.100(9)
Zn(2)−Cl(2)	2.235(3)	Zn(2b)−N(4b)	2.195(9)
Zn(2)−N(4)	2.253(9)	Zn(2b)−Cl(2b)	2.233(3)
Zn(2)−Cl(3)	2.410(3)	Zn(2b)−Cl(3b)	2.373(3)
Zn(1)−Zn(2)	3.374(2)	Zn(1b)−Zn(2b)	3.380(2)
N(1)−Zn(1)−O(1)	84.3(3)	N(1b)−Zn(1b)−O(1b)	82.0(3)
N(1)−Zn(1)−N(3)	80.6(3)	N(1b)−Zn(1b)−N(3b)	82.9(3)
O(1)−Zn(1)−N(3)	157.2(3)	O(1b)−Zn(1b)−N(3b)	155.3(3)
N(1)−Zn(1)−Cl(1)	115.0(2)	N(1b)−Zn(1b)−Cl(1b)	111.8(2)
O(1)−Zn(1)−Cl(1)	99.02(18)	O(1b)−Zn(1b)−Cl(1b)	99.30(18)
N(3)−Zn(1)−Cl(1)	102.8(2)	N(3b)−Zn(1b)−Cl(1b)	104.4(2)
N(1)−Zn(1)−Cl(3)	131.1(2)	N(1b)−Zn(1b)−Cl(3b)	133.7(2)
O(1)−Zn(1)−Cl(3)	80.3(2)	O(1b)−Zn(1b)−Cl(3b)	80.0(2)
N(3)−Zn(1)−Cl(3)	96.9(2)	N(3b)−Zn(1b)−Cl(3b)	96.8(3)
Cl(1)−Zn(1)−Cl(3)	113.10(13)	Cl(1b)−Zn(1b)−Cl(3b)	113.05(15)
N(2)−Zn(2)−O(1)	83.7(3)	O(1b)−Zn(2b)−N(2b)	84.9(3)
N(2)−Zn(2)−Cl(2)	105.0(3)	O(1b)−Zn(2b)−N(4b)	150.7(3)
O(1)−Zn(2)−Cl(2)	104.10(19)	N(2b)−Zn(2b)−N(4b)	79.5(4)
N(2)−Zn(2)−N(4)	82.7(4)	O(1b)−Zn(2b)−Cl(2b)	104.22(19)
O(1)−Zn(2)−N(4)	149.7(3)	N(2b)−Zn(2b)−Cl(2b)	106.2(2)
Cl(2)−Zn(2)−N(4)	105.6(2)	N(4b)−Zn(2b)−Cl(2b)	103.9(3)
N(2)−Zn(2)−Cl(3)	142.4(3)	O(1b)−Zn(2b)−Cl(3b)	79.9(2)
O(1)−Zn(2)−Cl(3)	79.5(2)	N(2b)−Zn(2b)−Cl(3b)	139.8(2)
Cl(2)−Zn(2)−Cl(3)	111.51(12)	N(4b)−Zn(2b)−Cl(3b)	96.3(3)
N(4)−Zn(2)−Cl(3)	95.3(3)	Cl(2b)−Zn(2b)−Cl(3b)	113.52(14)
Zn(1)−Cl(3)−Zn(2)	90.05(13)	Zn(1b)−Cl(3b)−Zn(2b)	91.60(13)
Zn(2)−O(1)−Zn(1)	109.0(4)	Zn(2b)−O(1b)−Zn(1b)	108.2(3)

It is unlikely that in zinc complexes with Schiff-base-type ligands the metal center(s) are involved in the redox process with regard to the two-electron oxidation of 3,5-DTBC, as proposed for the copper system. The EPR study at 77 K, performed immediately after mixing the Zn^{II} complex with 3,5-DTBC in an inert atmosphere, disclosed the possible cause of the redox process. Figure 11a and 11b for **2** and **5** (as representative for di- and mononuclear complexes, respectively) shows a broad, nearly isotropic EPR signal at $g \approx 2.00$.
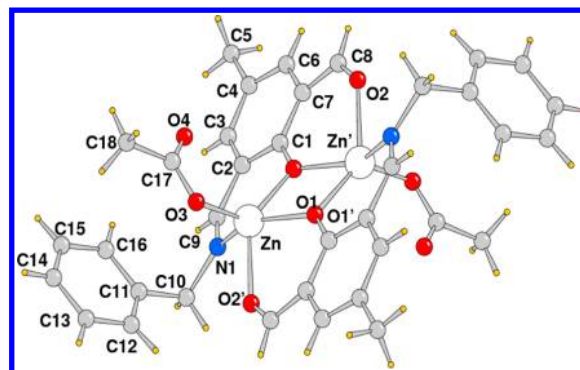
Figure 3. Molecular structure of complex cation of **4**.

Table 5. Coordination Bond Distances (Angstroms) and Angles (degrees) for Compound 4[a]

Zn−O(3)	1.981(4)	Zn−O(2′)	2.115(4)
Zn−O(1)	2.044(3)	Zn−N(1)	2.061(4)
Zn−O(1′)	2.063(3)	Zn−Zn′	3.2647(1)
O(3)−Zn−O(1)	128.16(16)	N(1)−Zn−O(1′)	144.57(15)
O(3)−Zn−N(1)	111.94(18)	O(3)−Zn−O(2′)	91.40(18)
O(1)−Zn−N(1)	87.93(15)	O(1)−Zn−O(2′)	137.72(15)
O(3)−Zn−O(1′)	102.98(17)	N(1)−Zn−O(2′)	90.10(17)
O(1)−Zn−O(1′)	74.71(13)	O(1′)−Zn−O(2′)	83.08(15)
Zn−O(1)−Zn′	105.29(13)		

[a]Primed atoms at $-x, -y + 1, -z + 1$.
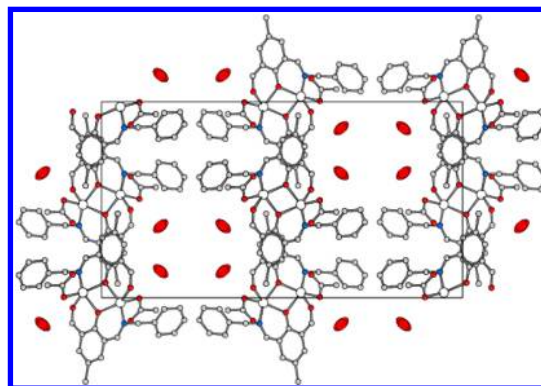
Figure 4. Crystal packing of complex **4** viewed down the *c* axis. Lattice water molecules (as ellipsoids) are shown in the channels.
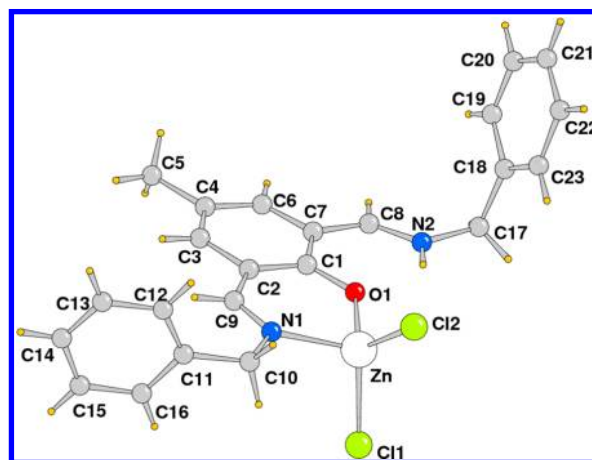
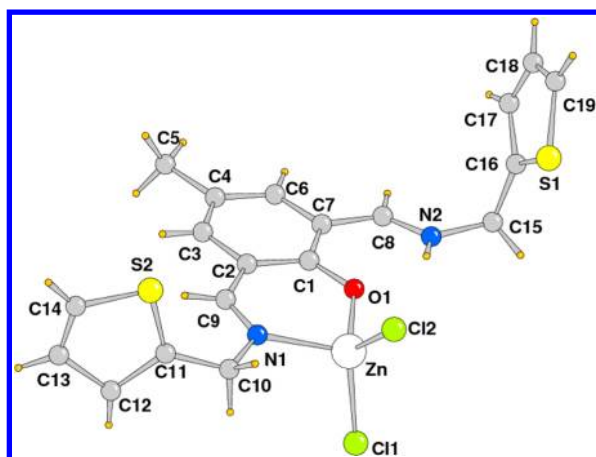**Figure 5.** Molecular structure with atom-numbering scheme of complex **5**.

Figure 6. Molecular structure with atom-numbering scheme of complex **6**.
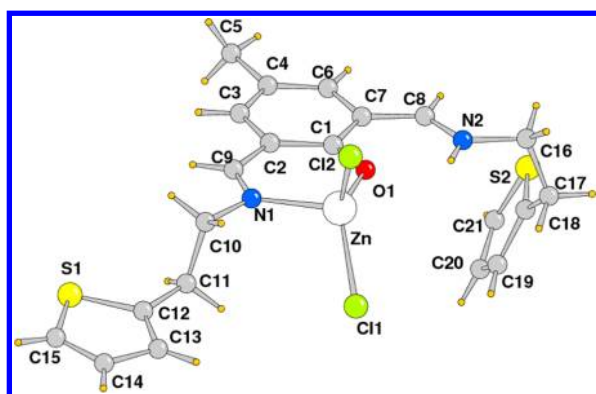

Figure 7. Molecular structure with atom-numbering scheme of complex **7**.

Table 6. Coordination Bond Distances (Angstroms) and Angles (degrees) for Complexes 5−7

	5	6	7
Zn−O(1)	1.958(6)	1.956(3)	1.9644(18)
Zn−N(1)	2.032(9)	2.057(4)	2.055(2)
Zn−Cl(1)	2.225(4)	2.2186(14)	2.2360(8)
Zn−Cl(2)	2.226(3)	2.2163(15)	2.2185(9)
O(1)−Zn−N(1)	91.9(3)	92.54(15)	91.75(9)
O(1)−Zn−Cl(1)	111.3(2)	108.86(11)	115.22(7)
N(1)−Zn−Cl(1)	105.3(3)	106.69(13)	106.00(7)
O(1)−Zn−Cl(2)	119.8(2)	116.37(11)	117.12(7)
N(1)−Zn−Cl(2)	105.3(3)	105.47(13)	104.90(7)
Cl(1)−Zn−Cl(2)	118.19(12)	122.08(6)	117.02(4)

Control experiments, in identical experimental conditions, show that all Zn^{II} complexes, as well as a mixture of Zn salts and 3,5-DTBC, are EPR silent. Thus, the EPR signal, which is a definite indication of formation of some ligand-centered radical species, is generated only when the Zn^{II} complex is mixed with 3,5-DTBC, and radical formation is most likely responsible for that oxidation. Critical analysis of the EPR spectra at 77 K at power saturation condition exhibited a characteristic weak half field signal at $g = 4.0$ (Supporting Information, Figure S40), indicating formation of two almost non-interacting radical centers in the triplet state. Formation of the triplet radical intermediate may be attributed to formation of two radicals; one at the ligand-centered imine radical, and another on the
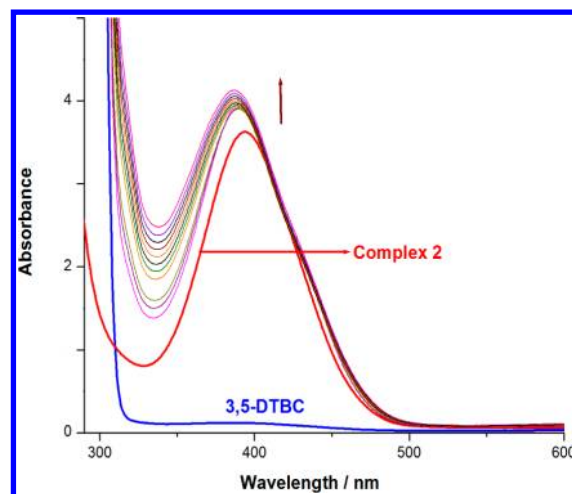

Figure 8. UV−vis spectra of (i) **2**, (ii) 3,5-DTBC, and (iii) changes in UV−vis spectra of **2** upon addition of 3,5-DTBC.
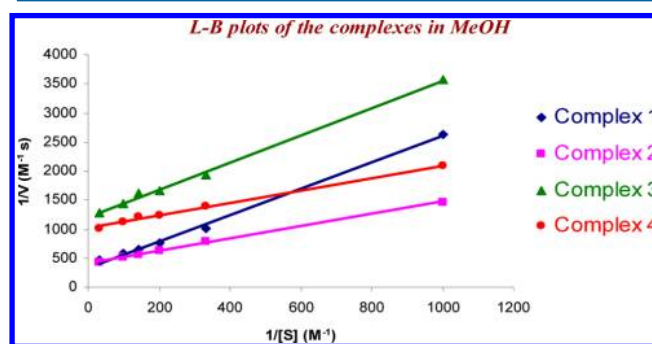

Figure 9. Lineweaver−Burk plots (double-reciprocal plot) for complexes **1−4** in methanol medium.

Table 7. Kinetics Data for Complexes 1−4

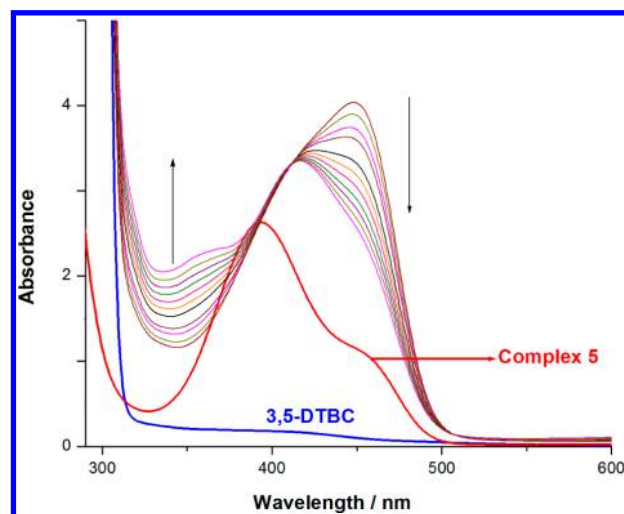| complex	wavelength (nm)	V_{max} (M s^{-1})	K_M (M)	k_{cat} (h^{-1})
1	395	2.96×10^{-3}	6.71×10^{-3}	1.06×10^{4}
2	386	2.45×10^{-3}	2.62×10^{-3}	8.82×10^{3}
3	389	8.25×10^{-4}	1.93×10^{-3}	2.97×10^{3}
4	401	9.78×10^{-4}	1.05×10^{-3}	3.52×10^{3}

Figure 10. UV−vis spectra of (i) **5**, (ii) 3,5-DTBC, and (iii) changes in spectra of **5** upon addition of 3,5-DTBC.
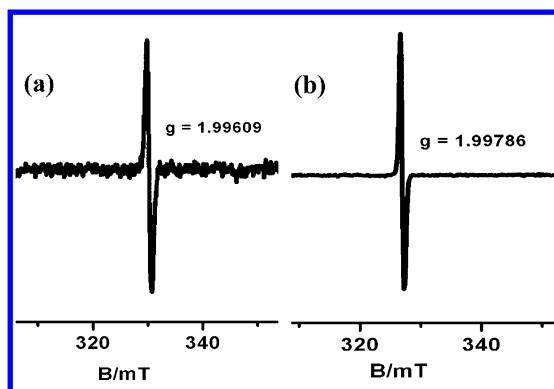
Figure 11. EPR spectra of the mixture of (a) **2** and 3,5-DTBC and (b) **5** and 3,5-DTBC.

substrate, i.e., semibenzoquinone radical. When the Zn^II complex is mixed with 3,5-DTBC, the imine bond of the coordinated ligand undergoes reduction with concomitant

oxidation of the catechol to form semibenzoquinone. The diradical situation in the above intermediate was further probed by the magnetic susceptibility measurement in solution following the Evans method (cf. Supporting Information). The effective magnetic moment μ_{eff} = 2.42 μ_B was observed, indicating that the intermediate formed upon mixing of 1 equiv of Zn^II complex with 3,5-DTBC is two-electron paramagnetic. This reaction was also followed in the presence of a radical scavenger, TEMPO (TEMPO = 2,2,6,6-tetramethylpiperidi-noxyl). Notably, no oxidation of catechol is detected spectroscopically (Supporting Information, Figure S35) in the presence of 2 equiv of TEMPO with respect to the catalyst used. This result gives further support that the catechol oxidation catalyzed by the reference Zn^II complexes is triggered by radical generation.

Moreover, in the catalytic reaction, when performed in an inert atmosphere, no 3,5-DTBQ formation has been observed. However, upon exposure of the reaction mixture in dioxygen atmosphere immediately 3,5-DTBQ formation was noticed. This observation indeed indicates that dioxygen is one of the
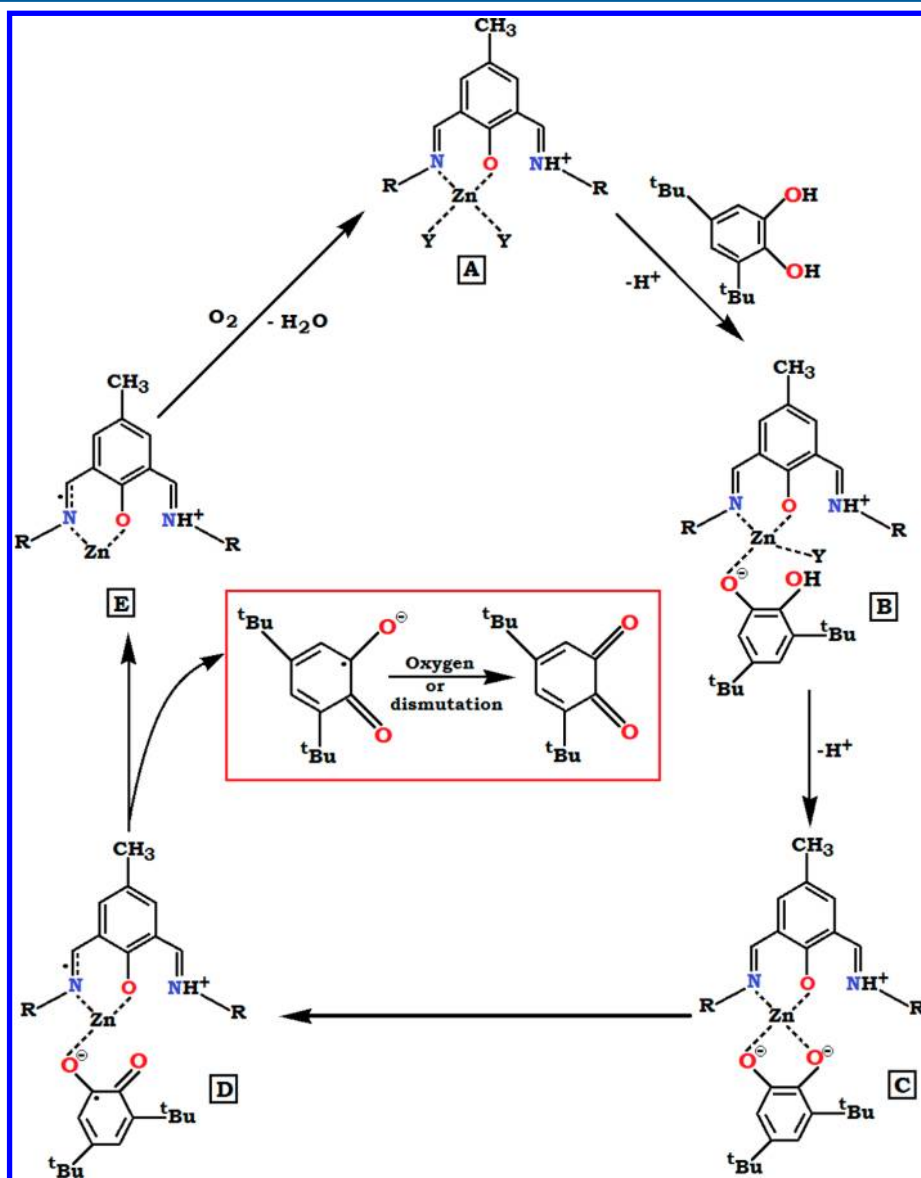

Figure 12. Proposed mechanism for the catalytic cycle of oxidation of 3,5-DTBC by mononuclear Zn(II) complexes.

active participants in the catalytic cycle; it converts the semibenzoquinone radical, formed in the first step of catalysis, to the quinone with subsequent regeneration of the catalyst. On the basis of the above experimental findings a plausible mechanism has been proposed in Figure 12. With the dinuclear complexes two catechol molecules are oxidized per cycle, whereas only one is oxidized by the monometallic Zn^{II} complexes.

In the voltammogram of the binuclear complexes **1**−**4** show two irreversible reduction peaks in the potential range from −0.6 to −1.4 V, while the mononuclear complexes **5**−**7** exhibit one irreversible reduction peak in the potential range from −0.75 to −1.0 V. Cyclic voltammograms of the two representative complexes **2** and **5** are displayed in Figure 13,
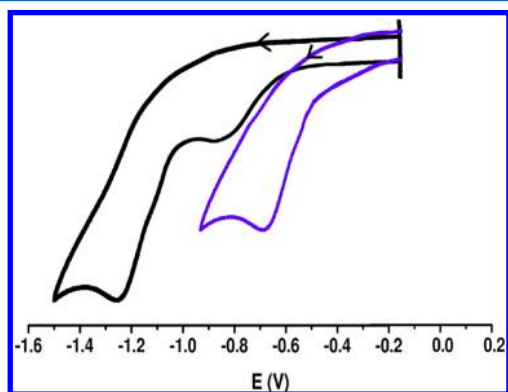

Figure 13. Cyclic voltammograms of complex **2** (black) and **5** (blue) in CH_2Cl_2/0.1 M Bu_4NClO_4 with platinum as the working electrode and saturated Ag/AgCl as the reference electrode.

and that of the other complexes are reported as Supporting Information (Figures S22 and S23). Since Zn^{II} is redox innocent, the process is attributable to reduction of the ligand backbone, presumably with formation of an imine radical, as reported by other groups with similar systems.[35]

DFT Calculations. In order to get a better understanding of the nature of the radical formed during catalysis we carried out DFT analysis. Calculations have been performed on the representative complexes **2** and **5** and on the corresponding one-electron-reduced analogues **2⁻** and **5⁻** at the B3LYP level using the Gaussian 03 software package. The structures of **2** and **5** proved to be the closed-shell singlet state with optimized structural parameters fully consistent with crystallographic data (see Supporting Information). The one-electron-reduced monoanionic species **2⁻** and **5⁻** display a doublet ($S = 1/2$) ground state, and the changes in net spin density (Figure 14) clearly indicate a ligand-centered process for the reductive reaction. In fact, the computational approach shows a significant elongation of the C=N imine bond in the monoanionic complexes (by 0.038 and 0.065 Å in **2⁻** and **5⁻**, respectively, compared to native species, see Supporting Information), indicating an imine radical ligand. The second electron reduction (for **2**) is again a ligand-based process, and the central Zn^{II} ions remain essentially invariant in all redox processes.

CONCLUSIONS

In this paper we studied the catecholase-like activity of seven Zn^{II} complexes (four di- and three mononuclear complexes) of phenol-based compartmental ligands using 3,5-DTBC as a
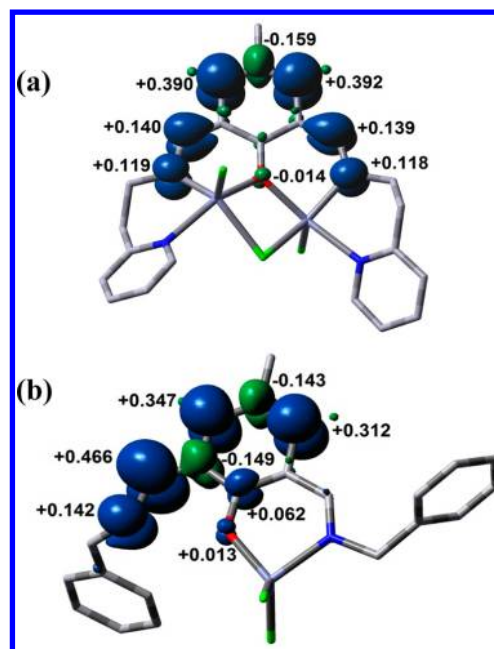

Figure 14. Spin density plots of (a) **2⁻** and (b) **5⁻**.

model substrate with the aim to assess the viability of the radical pathway in this catalytic process. All complexes are observed to be highly active in catalyzing the aerobic oxidation of 3,5-DTBC to 3,5-DTBQ. The mononuclear complexes (**5**−**7**) catalyze conversion of 3,5-DTBC to 3,5-DTBQ via formation of two enzyme−substrate adducts, whereas no such adduct has been detected by UV−vis spectrophotometric study in the conversion catalyzed by dinuclear complexes. The EPR experiment clearly shows generation of ligand radical complexes in the presence of 3,5-DTBC, and the cyclic voltammetric study also strengthens these findings, indicating the viability of the radical pathway in catecholase activity for these complexes. Alternative rationalization, such as metal-centered redox participation, does not look appropriate in redox-innocent Zn^{II} systems. Experimental results are corroborated by DFT analyses that confirm a ligand-centered radical in the reduced complexes with elongation of the imine bond length.

ASSOCIATED CONTENT

Ⓢ Supporting Information

X-ray crystallographic data in CIF format of complexes **1**−**7**; IR, ^{1}H NMR, ESI-MS, CV, UV−vis spectroscopic and kinetic data; results of DFT calculations. This material is available free of charge via the Internet at http://pubs.acs.org.

AUTHOR INFORMATION

Corresponding Author
*E-mail: dasdebasis2001@yahoo.com.

Notes

The authors declare no competing financial interest.

ACKNOWLEDGMENTS

■ REFERENCES

(1) (a) Solomon, E. I.; Sundaramand, U. M.; Machonkin, T. E. *Chem. Rev.* **1996**, *96*, 2563−2605. (b) Gerdemann, C.; Eicken, C.; Krebs, B. *Acc. Chem. Res.* **2002**, *35*, 183−191. (c) Koval, I. A.; Gamez, C.; Belle, P. G.; Reedijk, K. *Chem. Soc. Rev.* **2006**, *35*, 814−840.

(2) Neves, A.; Rossi, L. M.; Bortoluzzi, A. J.; Szpoganicz, B.; Wiezbicki, C.; Schwingel, E. *Inorg. Chem.* **2002**, *41*, 1788−1794.

(3) Triller, M. U.; Pursche, D.; Hsieh, W. Y.; Pecoraro, V. L.; Rompel, A.; Krebs, B. *Inorg. Chem.* **2003**, *42*, 6274−6283.

(4) Merkel, M.; Möller, N.; Piacenza, M.; Grimme, S.; Rompel, A.; Krebs, B. *Chem.—Eur. J.* **2005**, *11*, 1201−1209.

(5) Koval, I. A.; Belle, C.; Selmeczi, K.; Philouze, C.; Eric, S. A.; Schuitema, A. M.; Gamez, P.; Pierre, J. L.; Reedijk, J. *J. Biol. Inorg. Chem.* **2005**, *10*, 739−750.

(6) Murthy, N. N.; Mahroof-Tahir, M.; Karlin, K. D. *Inorg. Chem.* **2001**, *40*, 628−635.

(7) Belle, C.; Selmeczi, K.; Torelli, S.; Pierre, J.-L. *C. R. Chim.* **2007**, *10*, 271−283.

(8) Amudha, P.; Kandaswamy, M.; Govindasamy, L.; Velmurugan, D. *Inorg. Chem.* **1998**, *37*, 4486−4492.

(9) Mukherjee, J.; Mukherjee, R. *Inorg. Chim. Acta* **2002**, *337*, 429−438.

(10) Boxwell, C. J.; Bhalla, R.; Cronin, L.; Turner, S. S.; Walton, P. H. *J. Chem. Soc., Dalton Trans.* **1998**, 2449−2450.

(11) Banu, K. S.; Chattopadhyay, T.; Banerjee, A.; Bhattacharaya, S.; Suresh, E.; Nethaji, M.; Zangrando, E.; Das, D. *Inorg. Chem.* **2008**, *47*, 7083−7093.

(12) Banu, K. S.; Chattopadhyay, T.; Banerjee, A.; Mukherjee, M.; Bhattacharaya, S.; Patra, G. K.; Zangrando, E.; Das, D. *Dalton Trans.* **2009**, 8755−8764.

(13) Thompson, J. S.; Calabrese, J. C. *Inorg. Chem.* **1985**, *24*, 3167−3171.

(14) Kodera, M.; Kawata, T.; Kano, K.; Tachi, Y.; Itoh, S.; Kojo, S. *Bull. Chem. Soc. Jpn.* **2003**, *76*, 1957−1964.

(15) Siegbahn, P. E. M. *J. Biol. Inorg. Chem.* **2004**, *9*, 577−590.

(16) Mendoza-Quijano, M. R.; Ferrer-Sueta, G.; Flores-Álamo, M.; Aliaga-Alcalde, N.; Gómez-Vidales, V.; Ugalde-Saldívar, V. M.; Gasque, L. *Dalton Trans.* **2012**, *41*, 4985−4997.

(17) Chattopadhyay, T.; Mukherjee, M.; Mondal, A.; Maiti, P.; Banerjee, A.; Banu, K. S.; Bhattacharya, S.; Roy, B.; Chattopadhyay, D. J.; Mondal, T. K.; Nethaji, M.; Zangrando, E.; Das, D. *Inorg. Chem.* **2010**, *49*, 3121−3129.

(18) Guha, A.; Banu, K. S.; Banerjee, A.; Ghosh, T.; Bhattacharya, S.; Zangrando, E.; Das, D. *J. Mol. Catal. A: Chem.* **2011**, *338*, 51−57.

(19) (a) Bodini, M. E.; Copia, G.; Robinson, R.; Sawyer, D. T. *Inorg. Chem.* **1983**, *22*, 126−129. (b) Ruf, M.; Noll, B. C.; Groner, M. D.; Yee, G. T.; Pierpont, C. G. *Inorg. Chem.* **1997**, *36*, 4860−4865.

(20) Gagne, R. R.; Spiro, C. L.; Smith, T. J.; Hamann, C. A.; Thies, W. R.; Shiemeke, A. K. *J. Am. Chem. Soc.* **1981**, *103*, 4073−4081.

(21) (a) Evans, D. F. *J. Chem. Soc.* **1959**, 2003−2005. (b) Naklicki, M. L.; White, C. A.; Plante, L. L.; Evans, C. E. B.; Crutchley, R. J. *Inorg. Chem.* **1998**, *37*, 1880−1885. (c) Casabianca, B. L.; An, D.; Natarajan, K. J.; Roepe., D. P.; Wolf., C.; de Dios., C. A. *Inorg. Chem.* **2008**, *47*, 6077−6081.

(22) In *CRC Handbook of Chemistry and Physics*, 60th ed.; Weast, R. C., Astle, M. J., Eds.; CRC Press: Boca Raton, FL, 1980; p D-227.

(23) Drago, R. S. In *Physical Methods for Chemists*, 2nd ed.; Saunders College Publishing: Philadelphia, PA, 1992.

(24) Otwinowski, Z. W. In *Minor, Processing of X-ray Diffraction Data Collected in Oscillation Mode, Methods in Enzymology*; Carter, C. W.; Jr. Sweet, R. M., Eds.; Academic Press: New York, 1997; Vol. 276 (Macromolecular Crystallography, part A), pp 307−326.

(25) *SMART, SAINT. Software Reference Manual*; Bruker AXS Inc.: Madison, WI, 2000.

(26) In *SHELXL-97, Programs for Crystal Structure Analysis (Release 97-2)*; Sheldrick, G. M., Ed.; University of Göttingen: Germany, 1998.

(27) Farrugia, L. J. *J. Appl. Crystallogr.* **1999**, *32*, 837−838.

(28) Frisch, M. J.; Trucks, G. W.; Schlegel, H. B.; Scuseria, G. E.; Robb, M. A.; Cheeseman, J. R.; Montgomery, J. A., Jr.; Vreven, T.; Kudin, K. N.; Burant, J. C.; Millam, J. M.; Iyengar, S. S.; Tomasi, J.; Barone, V.; Mennucci, B.; Cossi, M.; Scalmani, G.; Rega, N.; Petersson, G. A.; Nakatsuji, H.; Hada, M.; Ehara, M.; Toyota, K.; Fukuda, R.; Hasegawa, J.; Ishida, M.; Nakajima, T.; Honda, Y.; Kitao, O.; Nakai, H.; Klene, M.; Li, X.; Knox, J. E.; Hratchian, H. P.; Cross, J. B.; Bakken, V.; Adamo, C.; Jaramillo, J.; Gomperts, R.; Stratmann, R. E.; Yazyev, O.; Austin, A. J.; Cammi, R.; Pomelli, C.; Ochterski, J. W.; Ayala, P. Y.; Morokuma, K.; Voth, G. A.; Salvador, P.; Dannenberg, J. J.; Zakrzewski, V. G.; Dapprich, S.; Daniels, A. D.; Strain, M. C.; Farkas, O.; Malick, D. K.; Rabuck, A. D.; Raghavachari, K.; Foresman, J .B.; Ortiz, J. V.; Cui, Q.; Baboul, A. G.; Clifford, S.; Cioslowski, J.; Stefanov, B. B.; Liu, G.; Liashenko, A.; Piskorz, P.; Komaromi, I.;Martin, R. L.; Fox, D. J.; Keith, T.;M. A. Al- LahamPeng, C. Y.; Nanayakkara, A.; Challacombe, M.; Gill, P. M. W.; Johnson, B.; Chen, W.; Wong, M. W.; Gonzalez, C.; Pople, J. A. *Gaussian 03*, Revision D.01; Gaussian, Inc.: Wallingford, CT, 2004.

(29) Becke, A. D. *Phys. Rev. A: At., Mol., Opt. Phys.* **1988**, *38*, 3098−3100.

(30) Lee, C.; Yang, W.; Parr, R. G. *Phys. Rev. B: Condens. Matter* **1988**, *37*, 785−789.

(31) (a) Stratmann, R. E.; Scuseria, G. E.; Frisch, M. J. *J. Chem. Phys.* **1998**, *109*, 8218−8224. (b) Casida, M. E.; Jamorski, C.; Casida, K. C.; Salahub, D. R. *J. Chem. Phys.* **1998**, *108*, 4439−4449.

(32) Compound **3** has been also reported by Roy, P.; Dhara, K.; Manassero, M.; Banerjee, P. *Inorg. Chim. Acta* **2009**, *362*, 2927−2932.

(33) Addison, A. W.; Rao, T. N.; Reedijk, J.; Vanrijn, J.; Verschoor, G. C. *J. Chem. Soc., Dalton Trans.* **1984**, 1349−1356.

(34) (a) Ye, B.-H.; Li, X.-Y.; Williams, I. D.; Chen, X.-M. *Inorg. Chem.* **2002**, *41*, 6426−6431. (b) Papaefstathiou, G. S.; Zhong, Z.; Geng, L.; Mac Gillivray, L. R. *J. Am. Chem. Soc.* **2004**, *126*, 9158−9159. (c) Abe, K.; Izumi, J.; Ohba, M.; Yokoyama, T.; Okawa, H. *Bull. Chem. Soc. Jpn.* **2001**, *74*, 85−95.

(35) (a) Lu, C. C.; Bill, E.; Weyhermüller, T.; Bothe, E.; Wieghardt, K. *J. Am. Chem. Soc.* **2008**, *130*, 3181−3197. (b) Bowman, A. C.; Milsmann, C.; Bill, E.; Lobkovsky, E.; Weyhermüller, T.; Wieghardt, K.; Chirik, P. J. *Inorg. Chem.* **2010**, *49*, 6110−6123.